# Au/epsilon-Fe2O3 Nanocomposites as Selective NO2 Gas Sensors

**ARTICLE** *in* THE JOURNAL OF PHYSICAL CHEMISTRY C · MAY 2014

Impact Factor: 4.77 · DOI: 10.1021/jp5032288



**8 AUTHORS**, INCLUDING:

Giorgio Carraro
University of Padova
**72** PUBLICATIONS **437** CITATIONS
SEE PROFILE

Elisabetta Comini
Università degli Studi di Brescia
**358** PUBLICATIONS **7,891** CITATIONS
SEE PROFILE

Alberto Gasparotto
University of Padova
**255** PUBLICATIONS **2,968** CITATIONS
SEE PROFILE

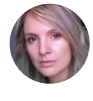

Cinzia Sada
University of Padova
**219** PUBLICATIONS **3,233** CITATIONS
SEE PROFILE

THE JOURNAL OF PHYSICAL CHEMISTRY C

Article

pubs.acs.org/JPCC

# Au/ε-$Fe_2O_3$ Nanocomposites as Selective $NO_2$ Gas Sensors

Daniel Peeters,[†,‡] Davide Barreca,[§] Giorgio Carraro,[†] Elisabetta Comini,[∥] Alberto Gasparotto,*[,†] Chiara Maccato,[†] Cinzia Sada,[⊥] and Giorgio Sberveglieri[∥]

[†]Department of Chemistry, Padova University and INSTM, 35131 Padova, Italy

[‡]Inorganic Materials Chemistry, Inorganic Chemistry 2, Ruhr-University Bochum, 44801 Bochum, Germany

[§]CNR-IENI and INSTM, Department of Chemistry, Padova University, 35131 Padova, Italy

[∥]SENSOR Lab, Department of Information Engineering, Brescia University and CNR-INO, 25133 Brescia, Italy

[⊥]Department of Physics and Astronomy, Padova University, 35131 Padova, Italy

Supporting Information

**ABSTRACT:** A combined chemical vapor deposition (CVD)/radio frequency (rf) sputtering approach to Au/$Fe_2O_3$ nanocomposites based on the scarcely investigated ε-iron(III) oxide polymorph is reported. The developed materials, analyzed by field emission-scanning electron microscopy (FE-SEM), energy dispersive X-ray spectroscopy (EDXS), X-ray photoelectron spectroscopy (XPS), and secondary ion mass spectrometry (SIMS), consisted of iron oxide nanorods decorated by gold nanoparticles (NPs), whose content and distribution could be tailored as a function of sputtering time. Interestingly, the intimate Au/ε-$Fe_2O_3$ interfacial contact along with iron oxide one-dimensional (1D) morphology resulted in promising performances for the selective detection of gaseous $NO_2$ at moderate working temperatures. At variance with the other iron(III) oxide polymorphs (α-, β-, and γ-$Fe_2O_3$), that display an *n*-type semiconducting behavior, ε-$Fe_2O_3$ exhibited a *p*-type response, clearly enhanced by Au introduction. As a whole, the obtained results indicate that the sensitization of *p*-type materials with metal NPs could be a valuable tool for the fabrication of advanced sensing devices.

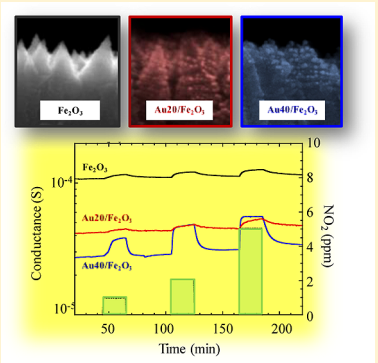


## INTRODUCTION

Metal oxide semiconductors (MOSs) have been extensively investigated as chemiresistive gas sensors. Applications in this field encompass environmental monitoring, fire detection, safety and medical devices, engines and combustion facilities, food quality control, and many other relevant areas.[1−4] In a MOS-based gas sensor, generally involving an *n*-type material, an electron depletion layer (EDL) forms upon molecular adsorption at the semiconductor surface, and a consequent electrical conductivity variation occurs. In this context, nanoscale materials are known to provide functional performances improved over the corresponding bulk ones, due to their higher surface area and defectivity, which favor an enhanced interaction with analyte gases.[1,2,5−8] Furthermore, as the grain size is reduced and becomes comparable to the EDL thickness, an increasing material fraction is influenced by adsorption/desorption processes and, as a whole, a higher sensitivity is achieved. Accordingly, MOS materials with a one-dimensional (1D) morphology, such as nanowires and nanotubes, are generally regarded as ideal building blocks for advanced sensing devices.[7,9−13]

Over the past decade, it has been reported that the decoration of MOS nanostructures with noble metal nanoparticles (NPs) can further enhance the sensor sensitivity and selectivity, resulting also in faster response/recovery time, as well as in lower operational temperatures.[8,9,14−16] These improved performances have been generally traced back to the catalytic activity of metal NPs, facilitating chemisorption of molecular oxygen and/or reactions involving the target gases.[1,9,17,18] Nevertheless, other phenomena, such as the formation of a Schottky barrier at the metal/oxide interface, yielding an improved charge carrier separation, also have to be taken into account.[7,13,18−20] Though the exact sensing mechanism is still a matter of debate, the morphology of the MOS matrix and metal NPs, as well as the chemical and electronic properties of the metal/oxide interface, play a key role in determining the overall system performances.[4,9,17,18,21] As a consequence, the development of versatile synthetic routes allowing a flexible control over these material features represents a crucial step.[14,15]

Among MOSs, iron(III) oxides present a remarkable applicative potential, thanks to their attractive chemico−physical properties coupled with their low toxicity and large availability. The two most common polymorphs, α-$Fe_2O_3$ (hematite) and γ-$Fe_2O_3$ (maghemite), have been used in different forms (films, nanoparticles, nanotubes, nanobelts, hierarchical structures, etc.) for gaseous analyte detection.[2,4,6,16,17,22] Recently, our group has demonstrated that

Received: April 1, 2014
Revised: May 7, 2014
Published: May 8, 2014

   dx.doi.org/10.1021/jp5032288 | J. Phys. Chem. C 2014, 118, 11813−11819

the rare and metastable $\varepsilon$-$Fe_2O_3$ phase is characterized by improved functional properties with respect to the widely used $\alpha$-$Fe_2O_3$ for photoassisted applications, thanks to its peculiar surface defectivity and electronic structure.[23−25] On this basis, the development of $\varepsilon$-$Fe_2O_3$-based gas sensors, eventually decorated with metal nanoparticles, can disclose interesting perspectives. It is worthwhile highlighting that, beyond conventional *n*-type materials, *p*-type MOSs, like the present $\varepsilon$-$Fe_2O_3$ nanosystems, have been recently proposed as gas sensors thanks to their inherent catalytic activity, surface reactivity, and electrical properties.[21,26,27]

On the basis of the above considerations, we report herein on a facile, green, and cost-effective preparative strategy to metal decorated $\varepsilon$-$Fe_2O_3$-based gas sensors. The approach consists of the CVD of the iron oxide matrix on a suitable substrate, followed by the controlled dispersion of Au NPs via rf-sputtering. The use of this hybrid synthetic route enables a direct integration of the sensing material into the device structure, thus avoiding any post-treatment procedure required to immobilize powdered systems.[10,12,13,16,28,29]

The prepared Au/$\varepsilon$-$Fe_2O_3$ systems have been tested in the detection of nitrogen dioxide ($NO_2$), a dangerous atmospheric pollutant derived from automobiles and industrial emissions, showing a high selectivity even at low working temperatures and a sensing behavior dependent on the Au NPs content and size.[3,10,11,27,30,31] To the best of our knowledge, this is the first report on the gas sensing properties of $\varepsilon$-$Fe_2O_3$-based materials available in the literature so far.

## EXPERIMENTAL SECTION

**Synthesis.** A cold-wall CVD horizontal apparatus was adopted for the synthesis of iron oxide deposits.[32,33] To this aim, $Fe(hfa)_2$TMEDA (hfa = 1,1,1,5,5,5-hexafluoro-2,4-pentanedionate; TMEDA = *N*,*N*,*N*′,*N*′-tetramethylethylenediamine), synthesized as previously reported,[34,35] was used as a molecular source and vaporized at 60 °C, setting growth temperature and total pressure to 400 °C and 10.0 mbar, respectively. Precursor vapors were transported toward the deposition zone by an $O_2$ flow (purity = 6.0; rate = 100 sccm) through heated gas lines to avoid condensation phenomena. An auxiliary oxygen flow (100 sccm) was also separately introduced into the reaction chamber after passing through a water reservoir maintained at 50 °C. Depositions were carried out for 60 min over 3 × 3 $mm^2$ Si(100) substrates covered by a 50-nm thick $SiO_2$ insulating layer (CRYSTAL GmbH, Berlin). Substrates were preliminarily subjected to a cleaning procedure consisting of immersion in water, washing with sulfonic detergent, and final rinsing in water.

For nanocomposite fabrication, gold nanoparticles were sputtered on the above-described iron oxide samples by a custom-built radio frequency (rf, $\nu$ = 13.56 MHz) plasma-chemical reactor using electronic grade Ar (purity = 5.0) as plasma source.[8,12,13] To this aim, a gold target (0.3 mm thick; BAL-TEC AG, 99.99%) was fixed on the rf electrode, while $Fe_2O_3$ matrices were mounted on a second grounded electrode. Sputtering processes were carried out under the following conditions: deposition temperature = 60 °C; rf-power = 5 W; total pressure = 0.3 mbar; Ar flow rate = 10 sccm. After optimization of the processing parameters, experiment duration was set to 20 or 40 min to tailor the corresponding Au amount in the composite systems. The obtained samples along with a bare $Fe_2O_3$ matrix were finally annealed in air at 400 °C for 1 h to attain their thermal stabilization in view of functional tests. Hereafter, composite specimens will be labeled as **Au20/$Fe_2O_3$** or **Au40/$Fe_2O_3$** according to the gold sputtering time (20 or 40 min, respectively).

**Characterization.** 2D X-ray microdiffraction ($XRD^2$) measurements were run in reflection mode on a Dymax-RAPID X-ray microdiffractometer, with a cylindrical imaging plate detector, which allows collecting from 0 to 160° ($2\theta$) horizontally and from −45 to +45° ($2\theta$) vertically upon using Cu K$\alpha$ radiation. Conventional XRD patterns were then obtained by integration of 2D images.

Field emission-scanning electron microscopy (FE-SEM) micrographs were collected by a Zeiss SUPRA 40VP instrument, using primary beam acceleration voltages of 10 kV. Line-scan energy dispersive X-ray spectroscopy (EDXS) analyses were carried out by monitoring the Fe K$\alpha$, O K$\alpha$, and Au L$\alpha$ signals throughout the deposit thickness by an Oxford INCA x-sight X-ray detector (acceleration voltage = 20.0 kV).

X-ray photoelectron spectroscopy (XPS) measurements were performed on a Thermo Scientific K-Alpha KA1066 spectrometer using a monochromatic Al K$\alpha$ X-ray source ($h\nu$ = 1486.6 eV). Photoelectrons were collected at a takeoff angle of 60°. A 400-$\mu$m diameter X-ray spot was used in the analyses. Charging correction was performed by assigning a binding energy (BE) of 284.8 eV to the adventitious C 1s signal. The estimated uncertainty on the reported BE values was ±0.2 eV.

Secondary ion mass spectrometry (SIMS) analyses were carried out by means of a IMS 4f mass spectrometer (Cameca) using a 14.5 keV $Cs^+$ primary beam (current = 20 nA) and by negative secondary ion detection, using an electron gun for charge compensation. Beam blanking mode and high mass resolution configuration were adopted. Signals were recorded rastering over a 150 × 150 $\mu m^2$ area, detecting secondary ions from a subregion close to 7 × 7 $\mu m^2$ to avoid crater effects. To take into account the dependence of the erosion rate on the matrix composition, the former was estimated at various depths by measuring the corresponding crater heights through a Tencor Alpha Step profiler.

For gas sensing experiments, platinum interdigitated contacts were deposited on the nanocomposite surfaces, whereas a platinum heating element was evaporated on the substrate backside. The flow-through technique was used for the characterization of gas sensing properties. The carrier gas was humid synthetic air (flow rate = 0.3 L/min, RH = 40%, temperature = 20 °C). A detailed description of the experimental setup and the contact geometry has already been reported.[29] The desired analyte concentrations were obtained from certified bottles and a mixing system equipped with mass flow controllers. Following the literature,[8] the sensor response for a *p*-type semiconductor exposed to an oxidizing gas was defined as the relative conductance variation ($S = (G_f - G_0)/G_0 = \Delta G/G_0$), where $G_0$ is the baseline conductance measured in air flow, and $G_f$ is the corresponding steady state value upon gas exposure. Response and recovery times are defined as the time to reach 90% of $G_f - G_0$ when the gas is introduced and to recover to 30% of the original conductance in air.[36]

## RESULTS AND DISCUSSION

On the basis of our recent publications,[24,37] the selective synthesis of $\varepsilon$-$Fe_2O_3$ was performed by CVD under the conditions reported in the Experimental Section. Processing parameters were optimized not only to avoid the formation of other iron(III) oxide polymorphs, but also to achieve a


dx.doi.org/10.1021/jp5032288 | J. Phys. Chem. C 2014, 118, 11813−11819

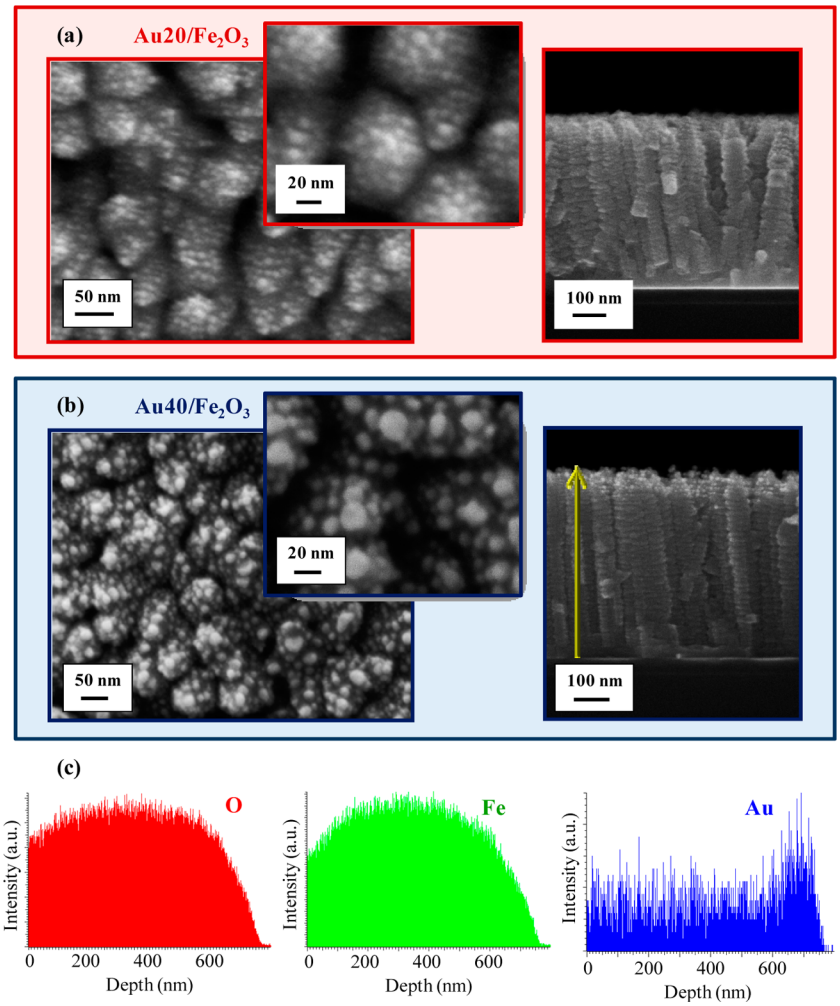


**Figure 1.** Plane-view (left) and cross-sectional (right) FE-SEM micrographs of samples (a) **Au20/$Fe_2O_3$** and (b) **Au40/$Fe_2O_3$**. (c) EDXS data collected along the yellow line marked in the cross-section of specimen **Au40/$Fe_2O_3$**. The arrow indicates the direction of abscissa increase.

columnar $\varepsilon$-$Fe_2O_3$ growth and obtain a porous oxide matrix (see Supporting Information (SI) Figures S1 and S2), to favor Au NPs dispersion. To this aim, Figure 1a and b displays the plane-view and cross-sectional FE-SEM micrographs of samples **Au20/$Fe_2O_3$** and **Au40/$Fe_2O_3$**, characterized by a gold sputtering time of 20 and 40 min, respectively. As a general rule, the pristine iron oxide morphology and crystallinity was preserved upon gold deposition thanks to the use of mild sputtering conditions.

As can be observed, the iron oxide matrix consist of a uniform array of nanorods (length = (540 ± 20) nm), oriented nearly perpendicular to the substrate surface. A statistical analysis of FE-SEM images allowed determination of average gold NP dimensions of (9 ± 2) and (13 ± 6) nm after 20 and 40 min of sputtering, respectively. The evolution of the particle size as a function of sputtering time suggested a 3-dimensional (Volmer−Weber) growth mode, as reported for Au deposition on various oxide and non-oxide supports.[38−41]

EDXS analyses were also carried out along the composites cross-section (Figure 1c). As can be observed, oxygen and iron signals exhibited a very similar profile, confirming the compositional homogeneity of the $Fe_2O_3$ matrix. Conversely, gold displayed a different in-depth distribution, suggesting that this element was mainly confined in the outermost sample region (≈ 100 nm).

The surface composition of the obtained systems was analyzed by XPS, devoting attention to the gold oxidation state and to the possible occurrence of any electronic interplay at the Au/$Fe_2O_3$ interface. Survey spectra (Figure 2) are

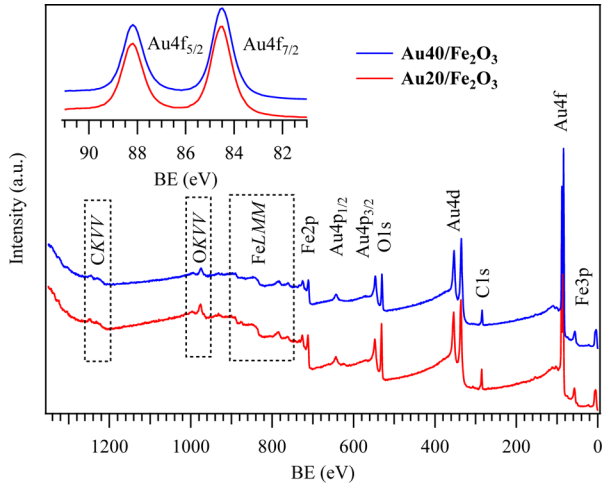


**Figure 2.** XPS survey spectra of Au/$\varepsilon$-$Fe_2O_3$ composites with different metal loadings. Au 4f photoelectron peaks are shown in the inset.


dx.doi.org/10.1021/jp5032288 | J. Phys. Chem. C 2014, 118, 11813−11819

dominated by the presence of iron, oxygen, and gold peaks, besides a relatively weak contribution from adventitious carbon (C 1s signal at 284.8 eV) due to atmospheric exposure. Irrespective of the synthetic conditions, the Fe 2p photoelectron peak presented two components, Fe $2p_{3/2}$ and Fe $2p_{1/2}$, with BEs of 711.1 and 724.8 eV, attributed to Fe(III) in $Fe_2O_3$ (SI Figure S3). The O 1s peak, centered at 530.1 eV, revealed the presence of lattice O in an iron(III) oxide environment, along with a high BE shoulder attributed to adsorbed −OH groups.[24] Regarding gold, its surface content increased with sputtering time from 32 to 43 at. %, whereas the Au $4f_{7/2}$ BE (Figure 2 inset) was 84.5 eV. Such a value, ca. 0.5 eV higher than the one usually detected for metallic gold,[8,14,15,38] could be due to the formation of a Schottky junction at the Au/$Fe_2O_3$ interface. Indeed, as also supported by gas sensing data (see below), the contact between *p*-type *ε*-$Fe_2O_3$ and gold NPs might result in an electron flow from the metal to the empty states of the MOS valence band, a phenomenon responsible for the gold peak shift on the high BE side.[41,42]

To obtain complementary information on the in-depth Au/$Fe_2O_3$ composition, SIMS analyses were carried out. In both specimens carbon content (not displayed) was in the range of 100−200 ppm, indicating a good sample purity. As can be observed in Figure 3, iron and oxygen ionic yields displayed a parallel trend throughout the investigated thickness, confirming the homogeneous composition of iron oxide matrices. After 70−80 min of erosion, the sudden decrease of iron and oxygen signals along with the parallel increase of the silicon one indicate the presence of a well-defined interface with the substrate. The overall sample thickness obtained by profilometry confirmed the values measured during cross-sectional FE-SEM analysis. Regarding gold, its presence was confined to the outermost sample region and its signal displayed an erfchian profile, as previously observed for other metal-containing oxide nanocomposites.[16,43] To this aim, a careful elaboration of SIMS data evidenced that gold was confined to the ca. 95 ± 10 nm surface region of specimens **Au20/$Fe_2O_3$** and **Au40/$Fe_2O_3$**.

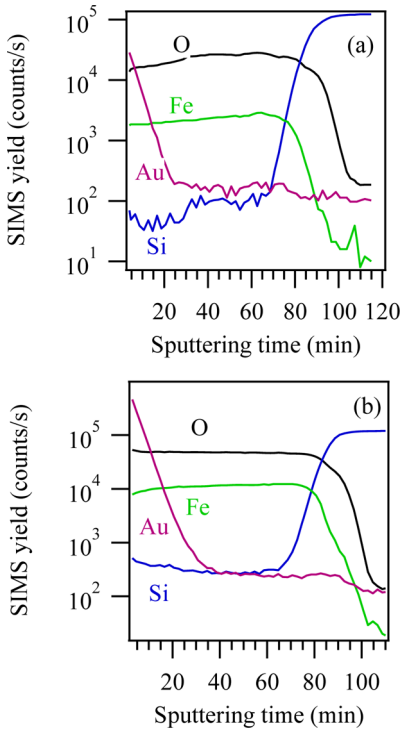


**Figure 3.** SIMS depth profiles of samples **Au20/$Fe_2O_3$** (a) and **Au40/$Fe_2O_3$** (b).

Finally, the gas sensing properties of the bare *ε*-$Fe_2O_3$ sample and the corresponding Au-decorated ones were investigated. Preliminary tests evidenced that all specimens were not sensitive to reducing species such as carbon monoxide, hydrogen, ethanol, and acetone, even at concentrations up to 500 ppm. Conversely, exposure to an oxidizing analyte, such as $NO_2$, resulted in a significant change of the sensor conductance, as displayed by Figure 4a. This behavior indicated a good selectivity of the obtained systems, a key advantage for practical applications.[8,43]

It is worthwhile to observe that, upon introduction of the analyte square concentration pulses, the highest conductance variations occurred for sample **Au40/$Fe_2O_3$**, characterized by the highest metal content. This phenomenon evidenced that gold NPs played a sensitizing role on the oxide matrix, in line with previous reports.[8,43] As can be noticed in Figure 4a, all sensors exhibited a conductance increase upon $NO_2$ exposure. Such an effect indicates that, at variance from the majority of MOS materials (including *α*-, *β*-, and *γ*-$Fe_2O_3$),[7,16,17,21,22] *ε*-$Fe_2O_3$ possesses a *p*-type behavior.

Though much less investigated than *n*-type systems, *p*-type oxides have recently attracted great attention for gas sensing applications due to their distinctive catalytic activity, surface reactivity, and electrical properties.[21,26,27] When a *p*-type oxide is exposed to air, oxygen molecules adsorb on its surface and ionize into species such as $O_2^-$, $O^-$, and $O^{2-}$ by collecting electrons from the semiconductor surface. Differently from *n*-type materials, for which the formation of an EDL occurs, for *p*-type systems like *ε*-$Fe_2O_3$ a hole accumulation layer (HAL) is generated. As a consequence, a low resistance surface layer is formed in this case, yielding, in turn, markedly different conduction patterns with respect to *n*-type semiconductors.[21,27]

When a *p*-type system is exposed to an oxidizing analyte such as $NO_2$, acting as an electron-trapping adsorbate, the following reactions take place:[11,27,44,45]

$$NO_{2(g)} + e^- \rightarrow {NO_2}^-_{(ads)} \quad (1)$$

$${NO_2}^-_{(ads)} + {O^-}_{(ads)} + 2e^- \rightarrow NO_{(g)} + 2O^{2-} \quad (2)$$

As a consequence, the HAL width (or hole concentration) increases further and a sensor conductance higher than the pristine air value is measured, as revealed by Figure 4a.

According to the literature, gold dispersion over iron oxide systems could improve the sensor behavior via either an electronic or chemical sensitization.[18−20] In the former case, the formation of a Schottky junction at the Au/$Fe_2O_3$ interface would result in an electron flow from the metal to *p*-type *ε*-$Fe_2O_3$. Compared to *ε*-$Fe_2O_3$, such a phenomenon, whose occurrence is also supported by the present XPS data, is expected to reduce the width of the HAL conduction channel in Au/$Fe_2O_3$ specimens, and hence decrease the corresponding conductance values in air, as actually observed (see Figure 4a and panels (i) and (ii) in Figure 4b). According to other authors, gold introduction could catalytically promote the dissociation of molecular oxygen (chemical sensitization), whose atomic products then diffuse to the metal oxide support.[17,19,20] Nevertheless, if a similar phenomenon was


dx.doi.org/10.1021/jp5032288 | J. Phys. Chem. C 2014, 118, 11813−11819

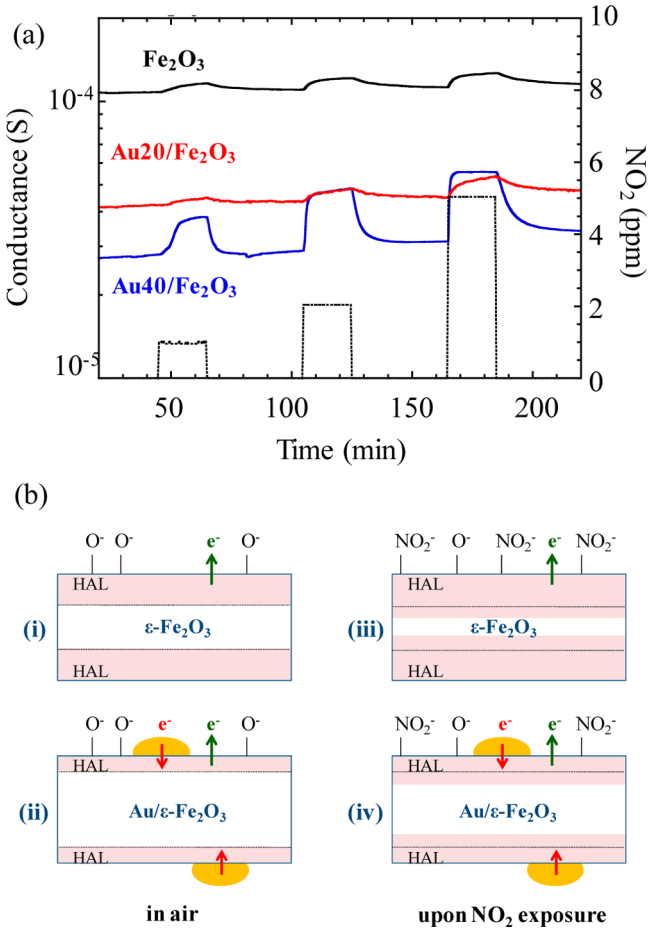


**Figure 4.** (a) Dynamic responses of $Fe_2O_3$-based samples to nitrogen dioxide square concentration pulses at a working temperature of 100 °C. (b) Schematic representation of the HAL thickness modulation in air (left) and in the presence of $NO_2$ (right) for bare and gold-decorated $\varepsilon$-$Fe_2O_3$ nanorods. Green arrows mark the directions of electron flow during $O_2$ or $NO_2$ chemisorption, whereas red arrows represent the electron flow from gold NPs (in yellow) to iron oxide due to the formation of a Schottky junction at the metal/oxide interface. (i) When $\varepsilon$-$Fe_2O_3$ is exposed to air, an HAL forms at the semiconductor surface. (ii) In the case of Au/$\varepsilon$-$Fe_2O_3$ exposure to air, electrons flow from the metal into the semiconductor due to the formation of a Schottky junction. This phenomenon reduces the HAL thickness and hence decreases the corresponding conductance value in air. Panels (iii) and (iv) represent (i) and (ii), respectively, after $NO_2$ exposure. In both cases an HAL expansion takes place but the effect is more marked for (iv) than for (iii). Hence, the relative conductance variation is higher in the latter case.

dominant over electronic sensitization, a trend of air conductance values opposite to that of Figure 4a would be expected. On the basis of the present results, it can be argued that gold mainly affects gas sensing performances via an electronic, rather than a chemical, mechanism. Consistently, such an effect can also explain the improved response of metal-containing samples to $NO_2$. Indeed, the relative conductance modulation occurring upon $NO_2$ exposure is expected to be enhanced for the initially thinner HAL region of Au/$\varepsilon$-$Fe_2O_3$ samples, in comparison to the bare $\varepsilon$-$Fe_2O_3$ (compare panels (iii) and (iv) in Figure 4b). The beneficial influence of gold NPs is also in line with the fact that **Au40/$Fe_2O_3$** exhibited the best response and recovery times (60 and 450 s, respectively, at 100 °C).

Figure 5 compares the responses of $\varepsilon$-$Fe_2O_3$ and Au/$\varepsilon$-$Fe_2O_3$ specimens to a representative nitrogen dioxide concentration,

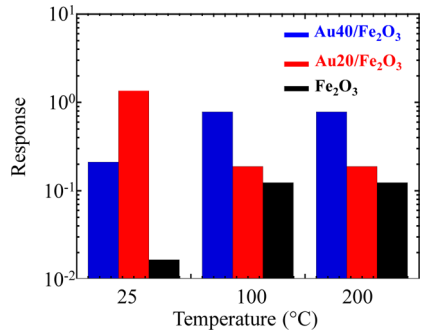


**Figure 5.** Response to 5 ppm of $NO_2$ as a function of the sensor working temperature for $\varepsilon$-$Fe_2O_3$ and Au/$\varepsilon$-$Fe_2O_3$ nanocomposites with different gold contents.

as a function of operating temperature. Irrespective of the sensor working conditions, bare iron oxide always displayed the worst performances, with a negligible response ($\leq 0.1$) at room temperature. Conversely, gold deposition resulted in an appreciable performance improvement already at 25 °C, a result of great interest in view of eventual practical applications. Whereas at 25 °C sample **Au20/$Fe_2O_3$** exhibited a response higher than **Au40/$Fe_2O_3$**, at 100 and 200 °C the opposite trend was detected, suggesting thus the occurrence of a change in the system sensitivity pattern.

It is generally accepted that response values are mainly restricted by the rate of chemical reactions and the diffusion of gas molecules, whose effects are predominant at low and high operating temperatures, respectively.[2,6] As a result of this counterbalance, optimal working conditions are typically achieved in the intermediate temperature regime. The different response vs temperature dependence of gold-containing samples can be traced back to the combined influence of two competitive effects, namely gold amount and particle size. While at 25 °C smaller, and hence more reactive, Au NPs appear to be important to promote the sensing process (compare SEM and XPS data for samples **Au20/$Fe_2O_3$** and **Au40/$Fe_2O_3$**), at higher temperatures the sensor mostly benefits from the increased metal content, likely corresponding to an higher density of Schottky nanojunctions (see the higher response for the **Au40/$Fe_2O_3$** specimen).

It is finally worth noticing that, since $NO_2$ strongly chemisorbs on many metal oxides, commercial sensors operate at 300−500 °C to enhance the surface molecular desorption kinetics.[45] Yet, such high temperatures are technologically unfavorable, since they result in a higher power consumption, reduced device lifetime, and lower operational safety, in particular in explosive environments.[8,26,45] As a consequence, the approach presented in this work for the fabrication of low-temperature $NO_2$ gas sensors possesses a strong applicative potential.

## CONCLUSIONS

In summary, we have presented herein the first report on the CVD/rf-sputtering fabrication of Au/$\varepsilon$-$Fe_2O_3$ composite materials as potential gas sensing platforms. More specifically, the unique features of the developed preparative strategy allowed the phase-selective synthesis of high purity $\varepsilon$-$Fe_2O_3$ nanorods and their surface decoration by Au NPs. Gas sensing


dx.doi.org/10.1021/jp5032288 | J. Phys. Chem. C 2014, 118, 11813−11819

tests evidenced that $\varepsilon$-$Fe_2O_3$ possesses a *p*-type behavior and functional performances clearly enhanced upon gold sensitization, along with a strong selectivity for the detection of $NO_2$ even at low operating temperatures. As a whole, the obtained findings candidate the present CVD/rf-sputtering approach as a versatile tool for the fabrication of advanced sensing devices for a variety of end-uses.

## ■ ASSOCIATED CONTENT

### Supporting Information

XRD pattern, plane-view, and cross-sectional FE-SEM micrographs; XPS Fe 2p and O 1s surface signals of $\varepsilon$-$Fe_2O_3$. This material is available free of charge via the Internet at http://pubs.acs.org.

## ■ AUTHOR INFORMATION

### Corresponding Author

*E-mail: alberto.gasparotto@unipd.it.

### Notes

The authors declare no competing financial interest.

## ■ ACKNOWLEDGMENTS

The research leading to these results has received funding from the European Community's Seventh Framework Program (FP7/2007-2013) under grant agreement ENHANCE-238409. We also kindly acknowledge the financial support under the FP7 project "SOLAROGENIX" (NMP4-SL-2012-310333), and from Padova University ex-60% 2012-2013 projects, PRAT 2010 (CPDA102579), grant CPDR132937/13 (SOLLEONE), and Regione Lombardia-INSTM ATLANTE projects. Thanks are also due to Prof. E. Bontempi (Brescia University, Italy), Prof. W. M. M. Kessels, and Dr. V. Longo (Eindhoven University of Technology, The Netherlands) for valuable assistance in sample characterization.

## ■ REFERENCES

(1) Vander Wal, R. L.; Berger, G. M.; Kulis, M. J.; Hunter, G. W.; Xu, J. C.; Evans, L. Synthesis Methods, Microscopy Characterization and Device Integration of Nanoscale Metal Oxide Semiconductors for Gas Sensing. *Sensors* **2009**, *9*, 7866−7902.

(2) Bandgar, D. K.; Navale, S. T.; Khuspe, G. D.; Pawar, S. A.; Mulik, R. N.; Patil, V. B. Novel Route for Fabrication of Nanostructured $\alpha$-$Fe_2O_3$ Gas Sensor. *Mater. Sci. Semicond. Proc.* **2014**, *17*, 67−73.

(3) Neri, G.; Bonavita, A.; Galvagno, S.; Siciliano, P.; Capone, S. CO and $NO_2$ Sensing Properties of Doped-$Fe_2O_3$ Thin Films Prepared by LPD. *Sens. Actuators, B* **2002**, *82*, 40−47.

(4) Neri, G.; Bonavita, A.; Galvagno, S.; Caputi, L.; Pacilè, D.; Marsico, R.; Papagno, L. HREELS Study of Au/$Fe_2O_3$ Thick Film Gas Sensors. *Sens. Actuators, B* **2001**, *80*, 222−228.

(5) Choi, S. W.; Jung, S. H.; Kim, S. S. Significant Enhancement of the $NO_2$ Sensing Capability in Networked $SnO_2$ Nanowires by Au Nanoparticles Synthesized via $\gamma$-Ray Radiolysis. *J. Hazard. Mater.* **2011**, *193*, 243−248.

(6) Navale, S. T.; Bandgar, D. K.; Nalage, S. R.; Khuspe, G. D.; Chougule, M. A.; Kolekar, Y. D.; Sen, S.; Patil, V. B. Synthesis of $Fe_2O_3$ Nanoparticles for Nitrogen Dioxide Gas Sensing Applications. *Ceram. Int.* **2013**, *39*, 6453−6460.

(7) Chen, C. Y.; Retamal, J. R. D.; Wu, I. W.; Lien, D. H.; Chen, M. W.; Ding, Y.; Chueh, Y. L.; Wu, C. I.; He, J. H. Probing Surface Band Bending of Surface-Engineered Metal Oxide Nanowires. *ACS Nano* **2012**, *6*, 9366−9372.

(8) Barreca, D.; Carraro, G.; Comini, E.; Gasparotto, A.; Maccato, C.; Sada, C.; Sberveglieri, G.; Tondello, E. Novel Synthesis and Gas Sensing Performances of CuO−$TiO_2$ Nanocomposites Functionalized with Au Nanoparticles. *J. Phys. Chem. C* **2011**, *115*, 10510−10517.

(9) Wang, S.; Zhang, H.; Wang, Y.; Wang, L.; Gong, Z. Facile One-Pot Synthesis of Au Nanoparticles Decorated Porous $\alpha$-$Fe_2O_3$ Nanorods for In Situ Detection of VOCs. *RSC Adv.* **2014**, *4*, 369−373.

(10) Van Tong, P.; Duc Hoa, N.; Van Quang, V.; Van Duy, N.; Van Hieu, N. Diameter Controlled Synthesis of Tungsten Oxide Nanorod Bundles for Highly Sensitive $NO_2$ Gas Sensors. *Sens. Actuators, B* **2013**, *183*, 372−380.

(11) Afzal, A.; Cioffi, N.; Sabbatini, L.; Torsi, L. $NO_x$ Sensors Based on Semiconducting Metal Oxide Nanostructures: Progress and Perspectives. *Sens. Actuators, B* **2012**, *171*−*172*, 25−42.

(12) Simon, Q.; Barreca, D.; Gasparotto, A.; Maccato, C.; Tondello, E.; Sada, C.; Comini, E.; Sberveglieri, G.; Banerjee, M.; Xu, K.; Devi, A.; Fischer, R. A. CuO/ZnO Nanocomposite Gas Sensors Developed by a Plasma-Assisted Route. *ChemPhysChem* **2012**, *13*, 2342−2348.

(13) Simon, Q.; Barreca, D.; Gasparotto, A.; Maccato, C.; Tondello, E.; Sada, C.; Comini, E.; Devi, A.; Fischer, R. A. Ag/ZnO Nanomaterials as High Performance Sensors for Flammable and Toxic Gases. *Nanotechnology* **2012**, *23*, 025502/1−025502/7.

(14) Zhang, J.; Liu, X.; Wang, L.; Yang, T.; Guo, X.; Wu, S.; Wang, S.; Zhang, S. Au-Functionalized Hematite Hybrid Nanospindles: General Synthesis, Gas Sensing and Catalytic Properties. *J. Phys. Chem. C* **2011**, *115*, 5352−5357.

(15) Zhang, J.; Liu, X.; Guo, X.; Wu, S.; Wang, S. A General Approach to Fabricate Diverse Noble-Metal (Au, Pt, Ag, Pt/Au)/$Fe_2O_3$ Hybrid Nanomaterials. *Chem.—Eur. J.* **2010**, *16*, 8108−8116.

(16) Carraro, G.; Barreca, D.; Comini, E.; Gasparotto, A.; Maccato, C.; Sada, C.; Sberveglieri, G. Controlled Synthesis and Properties of $\beta$-$Fe_2O_3$ Nanosystems Functionalized with Ag or Pt Nanoparticles. *CrystEngComm* **2012**, *14*, 6469−6476.

(17) Gunawan, P.; Mei, L.; Teo, J.; Ma, J.; Highfield, J.; Li, Q.; Zhong, Z. Ultrahigh Sensitivity of Au/1D $\alpha$-$Fe_2O_3$ to Acetone and the Sensing Mechanism. *Langmuir* **2012**, *28*, 14090−14099.

(18) Wang, C.; Yin, L.; Zhang, L.; Xiang, D.; Gao, R. Metal Oxide Gas Sensors: Sensitivity and Influencing Factors. *Sensors* **2010**, *10*, 2088−2106.

(19) Van Duy, N.; Duc Hoa, N.; Van Hieu, N. Effective Hydrogen Gas Nanosensor Based on Bead-Like Nanowires of Platinum-Decorated Tin Oxide. *Sens. Actuators, B* **2012**, *173*, 211−217.

(20) Kolmakov, A.; Klenov, D. O.; Lilach, Y.; Stemmer, S.; Moskovits, M. Enhanced Gas Sensing by Individual $SnO_2$ Nanowires and Nanobelts Functionalized with Pd Catalyst Particles. *Nano Lett.* **2005**, *5*, 667−673.

(21) Kim, H.-J.; Lee, J.-H. Highly Sensitive and Selective Gas Sensors Using *p*-Type Oxide Semiconductors: Overview. *Sens. Actuators, B* **2014**, *192*, 607−627.

(22) Rezlescu, E.; Doroftei, C.; Rezlescu, N.; Popa, P. D. Preparation, Structure and Gas-Sensing Properties of $\gamma$-$Fe_2O_3$ and $\gamma$-$Fe_2O_3$−$TiO_2$ Thick Films. *Phys. Status Solidi A* **2008**, *205*, 1790−1793.

(23) Barreca, D.; Carraro, G.; Gasparotto, A.; Maccato, C.; Rossi, F.; Salviati, G.; Tallarida, M.; Das, C.; Fresno, F.; Korte, D.; Lavrenčič Štangar, U.; Franko, M.; Schmeisser, D. Surface Functionalization of Nanostructured $Fe_2O_3$ Polymorphs: from Design to Light-Activated Applications. *ACS Appl. Mater. Interfaces* **2013**, *5*, 7130−7138.

(24) Carraro, G.; Maccato, C.; Bontempi, E.; Gasparotto, A.; Lebedev, O. I.; Turner, S.; Depero, L. E.; Van Tendeloo, G.; Barreca, D. Insights on Growth and Nanoscopic Investigation of Uncommon Iron Oxide Polymorphs. *Eur. J. Inorg. Chem.* **2013**, *2013*, 5454−5461.

(25) Carraro, G.; Maccato, C.; Gasparotto, A.; Montini, T.; Turner, S.; Lebedev, O. I.; Gombac, V.; Adami, G.; Van Tendeloo, G.; Barreca, D.; Fornasiero, P. Enhanced Hydrogen Production by Photoreforming of Renewable Oxygenates Through Nanostructured $Fe_2O_3$ Polymorphs. *Adv. Funct. Mater.* **2014**, *24*, 372−378.

(26) Barreca, D.; Bekermann, D.; Comini, E.; Devi, A.; Fischer, R. A.; Gasparotto, A.; Gavagnin, M.; Maccato, C.; Sada, C.; Sberveglieri, G.; Tondello, E. Plasma Enhanced-CVD of Undoped and Fluorine-Doped $Co_3O_4$ Nanosystems for Novel Gas Sensors. *Sens. Actuators, B* **2011**, *160*, 79−86.

(27) Wetchakun, K.; Samerjai, T.; Tamaekong, N.; Liewhiran, C.; Siriwong, C.; Kruefu, V.; Wisitsoraat, A.; Tuantranont, A.;

Phanichphant, S. Semiconducting Metal Oxides as Sensors for Environmentally Hazardous Gases. *Sens. Actuators, B* **2011**, *160*, 580−591.
(28) Eranna, G.; Joshi, B. C.; Runthala, D. P.; Gupta, R. P. Oxide Materials for Development of Integrated Gas Sensors: a Comprehensive Review. *Crit. Rev. Solid State Mater. Sci.* **2004**, *29*, 111−188.
(29) Barreca, D.; Gasparotto, A.; Maccato, C.; Maragno, C.; Tondello, E.; Comini, E.; Sberveglieri, G. Columnar $CeO_2$ Nanostructures for Sensor Application. *Nanotechnology* **2007**, *18*, 125502/1−125502/6.
(30) You, L.; He, X.; Wang, D.; Sun, P.; Sun, Y. F.; Liang, X. S.; Du, Y.; Lu, G. Y. Ultrasensitive and Low Operating Temperature $NO_2$ Gas Sensor Using Nanosheets Assembled Hierarchical $WO_3$ Hollow Microspheres. *Sens. Actuators, B* **2012**, *173*, 426−432.
(31) Tulliani, J. M.; Baroni, C.; Lopez, C.; Dessemond, L. New $NO_x$ Sensors Based on Hematite Doped with Alkaline and Alkaline-Earth Elements. *J. Eur. Ceram. Soc.* **2011**, *31*, 2357−2364.
(32) Barreca, D.; Gasparotto, A.; Maragno, C.; Tondello, E.; Sada, C. CVD of Nanophasic (Zn,Cd)S Thin Films: From Multi-layers to Solid Solutions. *Chem. Vap. Deposition* **2004**, *10*, 229−236.
(33) Barreca, D.; Gasparotto, A.; Maragno, C.; Tondello, E.; Bontempi, E.; Depero, L. E.; Sada, C. CVD of Lanthanum Oxyfluoride-Based Thin Films From a Lanthanum $\beta$-Diketonate Diglyme Precursor. *Chem. Vap. Deposition* **2005**, *11*, 426−432.
(34) Barreca, D.; Carraro, G.; Gasparotto, A.; Maccato, C.; Seraglia, R.; Tabacchi, G. An Iron(II) Diamine Diketonate Molecular Complex: Synthesis, Characterization and Application in the CVD of $Fe_2O_3$ Thin Films. *Inorg. Chim. Acta* **2012**, *380*, 161−166.
(35) Barreca, D.; Carraro, G.; Devi, A.; Fois, E.; Gasparotto, A.; Seraglia, R.; Maccato, C.; Sada, C.; Tabacchi, G.; Tondello, E.; Venzo, A.; Winter, M. $\beta$-$Fe_2O_3$ Nanomaterials from an Iron(II) Diketonate-Diamine Complex: a Study from Molecular Precursor to Growth Process. *Dalton Trans.* **2012**, *41*, 149−155.
(36) Barreca, D.; Bekermann, D.; Comini, E.; Devi, A.; Fischer, R. A.; Gasparotto, A.; Maccato, C.; Sberveglieri, G.; Tondello, E. 1-D ZnO Nano-Assemblies by Plasma-CVD as Chemical Sensors for Flammable and Toxic Gases. *Sens. Actuators, B* **2010**, *149*, 1−7.
(37) Carraro, G.; Barreca, D.; Maccato, C.; Bontempi, E.; Depero, L. E.; de Julián Fernández, C.; Caneschi, A. Supported $\varepsilon$ and $\beta$ Iron Oxide Nanomaterials by Chemical Vapor Deposition: Structure, Morphology and Magnetic Properties. *CrystEngComm* **2013**, *15*, 1039−1042.
(38) Armelao, L.; Barreca, D.; Gasparotto, A.; Pierangelo, E.; Tondello, E.; Polizzi, S. Preparation of Gold Nanoparticles on Silica Substrate by Radio Frequency Sputtering. *J. Nanosci. Nanotechnol.* **2005**, *5*, 259−265.
(39) Komsiyska, L.; Staikov, G. Electrocrystallization of Au Nanoparticles on Glassy Carbon from $HClO_4$ Solution Containing $[AuCl_4]^-$. *Electrochim. Acta* **2008**, *54*, 168−172.
(40) Barreca, D.; Gasparotto, A.; Tondello, E.; Bruno, G.; Losurdo, M. Influence of Process Parameters on the Morphology of Au/$SiO_2$ Nanocomposites Synthesized by Radio-Frequency Sputtering. *J. Appl. Phys.* **2004**, *96*, 1655−1665.
(41) Pan, Y.; Gao, Y.; Wang, G.; Kong, D.; Zhang, L.; Hou, J.; Hu, S.; Pan, H.; Zhu, J. Growth, Structure, and Stability of Au on Ordered $ZrO_2$(111) Thin Films. *J. Phys. Chem. C* **2011**, *115*, 10744−10751.
(42) Neamen, D. A. *An Introduction to Semiconductor Devices*; McGraw-Hill: New York, 2006.
(43) Barreca, D.; Comini, E.; Gasparotto, A.; Maccato, C.; Pozza, A.; Sada, C.; Sberveglieri, G.; Tondello, E. Vapor Phase Synthesis, Characterization and Gas Sensing Performances of $Co_3O_4$ and Au/$Co_3O_4$ Nanosystems. *J. Nanosci. Nanotechnol.* **2010**, *10*, 8054−8061.
(44) Barreca, D.; Bekermann, D.; Comini, E.; Devi, A.; Fischer, R. A.; Gasparotto, A.; Maccato, C.; Sada, C.; Sberveglieri, G.; Tondello, E. Urchin-Like ZnO Nanorod Arrays for Gas Sensing Applications. *CrystEngComm* **2010**, *12*, 3419−3421.
(45) Law, M.; Kind, H.; Messer, B.; Kim, F.; Yang, P. Photochemical Sensing of $NO_2$ with $SnO_2$ Nanoribbon Nanosensors at Room Temperature. *Angew. Chem., Int. Ed.* **2002**, *41*, 2405−2408.